ELSEVIER

Journal of Photochemistry and Photobiology A: Chemistry 101 (1996) 105–111

Journal of PHOTOCHEMISTRY AND PHOTOBIOLOGY A:CHEMISTRY

Mechanism of chlorine dioxide photodissociation in condensed media

M.A. Brusa, L.J. Perissinotti, M.S. Churio, A.J. Colussi *

Department of Chemistry, University of Mar del Plata, 7600 Mar del Plata, Argentina

Received 12 December 1995; accepted 29 February 1996

Abstract

The photobleaching of OClO dissolved in CCl_4 was investigated by kinetic electron spin resonance spectrometry as a function of [OClO], [O_2], photon flux, irradiation wavelength ($\lambda = 303$, 365 and 436 nm) and temperature ($233\ K \leq T \leq 298\ K$). OClO decays non-exponentially, the apparent kinetic order increasing with conversion. The initial quantum yields of OClO disappearance Φ are larger than one under anoxic conditions, but decrease in the presence of O_2, except at 365 nm. The rates are directly proportional to the absorbed photon flux and depend weakly on temperature. Remarkably, OClO is partially regenerated after irradiation, even in fully bleached solid samples. We show that a minimal mechanism comprising 21 pseudo-elementary steps can account for these observations, within experimental error, if the primary products of OClO photodecomposition change from (O + ClO) at 303 and 436 nm to (Cl + O_2) at 365 nm. The photolysis of $ClOClO_2$, one of the putative intermediate species, into (Cl + OClO) also contributes to the initial rates at 303 nm.

Keywords: Chlorine dioxide; Electron spin resonance; Kinetics; Ozone; Photodissociation

1. Introduction

The photodecomposition of chlorine dioxide (OClO) in the near-UV has recently received much attention due to its potential role in polar stratospheric ozone depletion [1–15]. In this regard, OClO is important if step (2)

$$OClO(X^2B_1) + h\nu \rightarrow OClO(^2A_2) \rightarrow ClO(X^2\Pi) + O(^3P) \quad (1)$$

$$OClO(X^2B_1) + h\nu \rightarrow Cl(^2P) + {}^{1,3}O_2 \quad (2)$$

occurs to any measurable extent because, although O atoms lead to a null cycle, Cl atoms initiate a long chain reaction which efficiently destroys ozone [7,11].

The importance of reaction (2) in the gas phase is minor; femtosecond probing and photofragment translational energy spectroscopy experiments reveal modest (less than 4%) Cl atom yields [2,3]. Larger Cl atom yields (greater than 15%) in resonantly enhanced multiphoton ionization (REMPI) action spectra studies of OClO at approximately 360 nm, can be ascribed to secondary photolysis of excited ClO primary fragments [6,11].

In contrast, a time-resolved study of OClO photodecomposition in water solution at 355 nm [1,9] and very recent results in carbon tetrachloride [15] and water solution are consistent with substantial Cl atom formation in condensed media [16]. These results are seemingly in line with previous experiments carried out in frozen inert matrices [17–19], in which OClO is quantitatively converted into its asymmetrical isomer ClOO, a species which readily decomposes into the products of reaction (2) at ambient temperature [20]. However, it should be realized that the photoisomerization of OClO in solid media as well as the formation of Cl atoms in inert solvents can conceivably derive from step (1) via a common route, i.e. process (I)

$$OClO + h\nu \rightarrow [O + ClO]_{cage} \rightarrow [ClOO] \rightarrow Cl + O_2 \quad (I)$$

taking place inside cages of dissimilar persistence [15]. The thermodynamically more stable isomer ClOO is expected to be the final species within an inescapable cavity at sufficiently low temperatures regardless of its mechanism of generation, i.e. whether it is formed by concerted isomerization or via steps (1) and/or (2) followed by association of the primary fragments.

In this paper, we report systematic electron spin resonance (ESR) measurements of the kinetics of OClO photobleaching in carbon tetrachloride solutions on stationary irradiation at 303, 365 and 436 nm in the presence and absence of O_2. In order to account for the measured absolute quantum yields, the non-exponential OClO decays and the post-illumination partial regeneration of OClO, it is necessary to invoke a

* Corresponding author. Tel.: +54 23 94 5525; fax: +54 23 91 9106; e-mail: colussi@mdp.edu.ar

PII S1010-6030(96)04347-X

scheme comprising well-established radical–radical and radical–molecule reactions, as well as a few radical equilibria. However, rationalization of the singular lack of O_2 kinetic effects at approximately 365 nm requires a qualitative change in the mode of OClO photofragmentation, because the non-monotonic wavelength dependence excludes a mechanism operating through excess kinetic energy delivered to the geminate radical pair [21,22]. We conjecture that this peculiar photoselectivity effect may be related to the mechanism underlying the solvatochromic red shifts observed in the near-UV spectrum of OClO, namely the coupling of molecular electronic excited states via dynamic electronic polarization of the solvent [23,24]. Quantum yields at 303 nm require an additional source of Cl atoms, which is provided by the photodecomposition of $ClOClO_2$, one of the transient species in this system [25].

2. Experimental details

Photolysis was carried out on liquid samples (volume, 136 μl) contained in silica tubes (internal diameter, 4 mm), located within the temperature-controlled, optical microwave cavity of a Bruker 220 X-band ESR spectrometer. The output of a 1000 W Hanovia Hg/Xe lamp, dispersed by a Czerny Turner high-intensity grating monochromator (Schoeffel-Kratos, ±5 nm resolution), fully illuminated the sample volume. Incident photon fluxes were determined in situ using a potassium ferrioxalate actinometer [26]; they were corrected for the variation of the optical path length resulting from the different refractive indices of water and carbon tetrachloride, and for partial light absorption by the actinometer at 436 nm (see Appendix A). Concentrated OClO stock solutions were prepared by passing Cl_2–N_2 or Cl_2–O_2 mixtures through moist $NaClO_2$, and bubbling the effluent gases into CCl_4 kept over $MgSO_4$. Dilute solutions (0.08–1.4 mM) were prepared from stock solutions and neat solvent under dry nitrogen or oxygen. Carbon tetrachloride (Erba, reagent) was purified through alumina, dried over $MgSO_4$ and finally distilled. Solutions, prepared daily and kept in the dark, were titrated for OClO using standard methods, which confirmed the presence of negligible amounts of Cl_2 (less than 1% of [OClO]). The spectra of such solutions yielded the following values of the OClO optical absorption cross-section σ (base e): $\sigma \times 10^{20}$ (cm^2 $molecule^{-1}$): 65.0 (436 nm), 389 (365 nm), 569 (363 nm, maximum) and 117 (303 nm) in CCl_4 at 298 K [15].

3. Results and discussion

3.1. Experimental observations

The ESR spectrum of OClO in CCl_4 consists of a broad signal displaying a largely unresolved quartet, even at the very low concentrations employed here ($g_{iso} = 2.1265$, $a_{iso}(^{35}Cl) = 1.31$ mT). The ClO_3 radical, another conceivably present species, has very different magnetic parameters ($g_{iso} = 2.006$, $a_{iso}(^{35}Cl) = 12.12$ mT), but was not detected at concentrations above 1 μM [27]. Other radicals, such as ClO, Cl and O, presumably present in our system, are orbitally degenerate and therefore ESR silent in condensed media [18]. Hence ESR signals are specific to OClO under the present conditions, a distinct advantage of paramagnetic resonance spectrometry over broad-band optical techniques used in previous studies. The first derivative ESR signals of steadily irradiated OClO solutions were measured as a function of time at fixed magnetic fields locked at their maxima, i.e. approximately 338.0 mT at 9.70 GHz. Signals were monitored for periods between 50 and 500 s depending on the photon flux.

Since the solvent absorbs radiation below $\lambda = 240$ nm, OClO is the only photochemically active species in this system at the beginning of the experiments. Initial OClO concentrations ($[OClO]_0$) were chosen to ensure that less than 20% of the incident photon flux is absorbed in the photolysis tubes at any wavelength, i.e. $[OClO]_0 \leq 1.6$ mM, 0.27 mM and 0.91 mM at 436, 365 and 303 nm respectively. The temporal evolution of the ESR signals on illumination is slower than exponential at all wavelengths in the presence or absence of O_2(g) (Figs. 1–3). Moreover, the signals partially recover after irradiation, even in the solid phase (Fig. 4). Both observations provide direct evidence of a complex mechanism, i.e. OClO not only disappears by photodissociation, but is also consumed in secondary reactions involving primary fragments.

It is instructive to begin with the kinetic analysis of this system at very small OClO conversions, where the role of secondary processes is kept to a minimum. This was accomplished by fitting decay curves by polynomials and evaluating their analytical derivatives at time zero, which provided the initial rates of OClO disappearance R_0. In Figs. 5–7, we present R_0 vs. $[OClO]_0$ data determined at 436, 365 and 303 nm

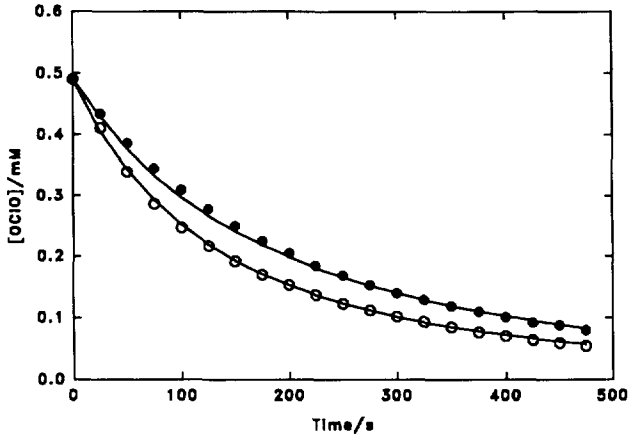

Fig. 1. [OClO] vs. time data at $\lambda = 436$ nm: ○, data obtained under 1 atm N_2; ●, data obtained under 1 atm O_2. Curves were calculated by integration of the mechanism given in Table 2. For this particular plot, the actual $[OClO]_0$ value under N_2 was scaled by a factor of 0.437 to allow direct comparison with the O_2 results.

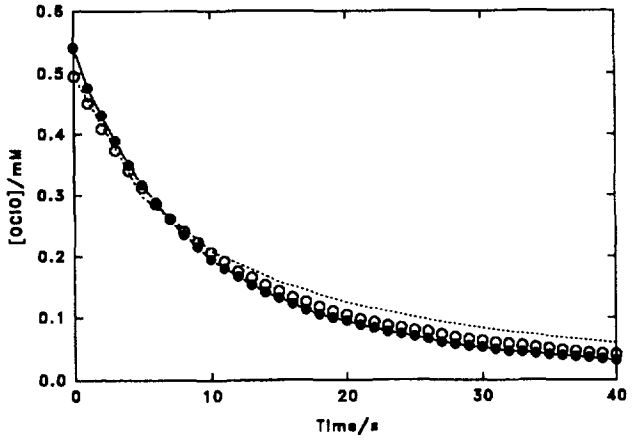

Fig. 2. Same as in Fig. 1, but at $\lambda = 365$ nm. The broken line is the simulation under 1 atm O_2.

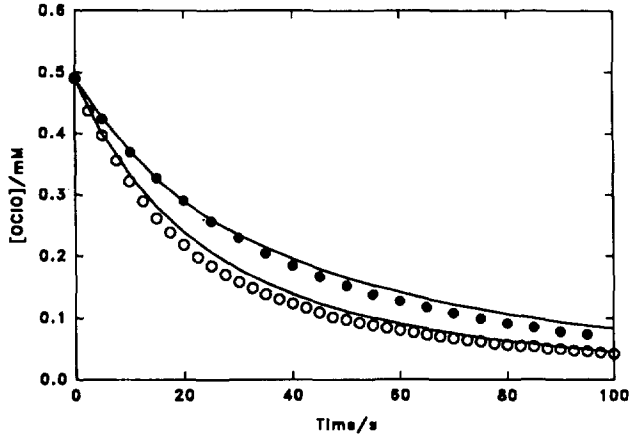

Fig. 3. Same as Fig. 1, but at $\lambda = 303$ nm.

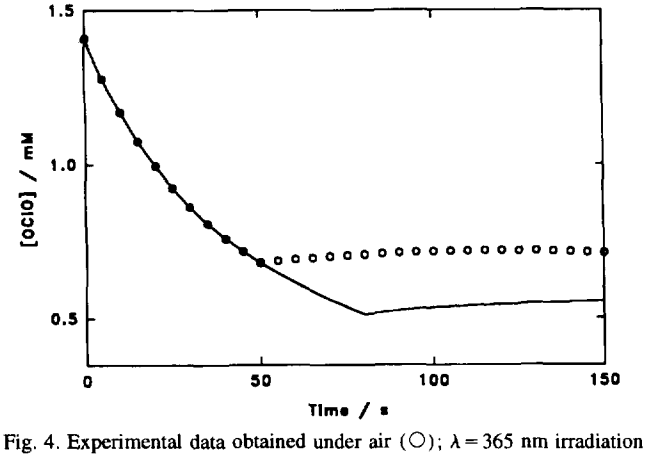

Fig. 4. Experimental data obtained under air (○); $\lambda = 365$ nm irradiation was interrupted at 50 s. The curve was obtained by integration of the mechanism given in Table 2, with illumination interrupted at the maximum of the calculated {[ClO] + [Cl]} values.

under either N_2 or O_2, which confirm the linear dependence; the slopes of these plots (k) have units of reciprocal time and depend on λ and $[O_2]$. The absolute initial quantum yields of OClO disappearance Φ can then be calculated from

$$\Phi = k[\mathrm{OClO}]_0 / I_a \qquad \text{(II)}$$

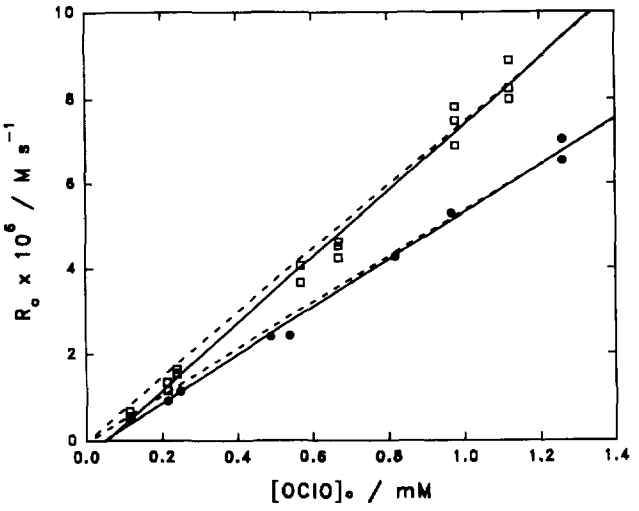

Fig. 5. Initial rates R_0 of OClO disappearance vs. $[\mathrm{OClO}]_0$ ($\lambda = 436$ nm): □, experimental data obtained under 1 atm N_2; ●, experimental data obtained under 1 atm O_2. Full lines correspond to unweighted first-order regressions. Broken lines were calculated using the mechanism described in Table 2 at 1% OClO conversion for $f = 2.70 \times 10^{-3}\ s^{-1}$ and $g = 1.56 \times 10^{-4}\ s^{-1}$.

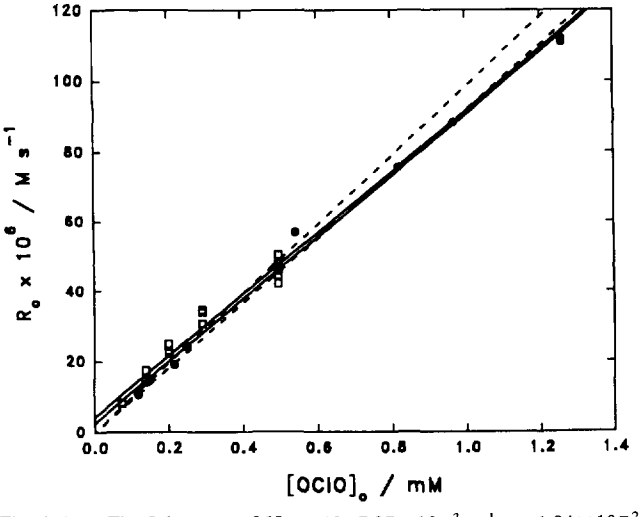

Fig. 6. As in Fig. 5, but at $\lambda = 365$ nm ($f = 7.27 \times 10^{-3}\ s^{-1}$, $g = 1.94 \times 10^{-2}\ s^{-1}$).

where $k[\mathrm{OClO}]_0 = R_0$ is the initial reaction rate ($M\ s^{-1}$) and I_a is the absorbed photon flux (einstein $l^{-1}\ s^{-1}$). I_a was calculated from the incident photon flux I_0, measured by a potassium ferrioxalate actinometer (0.15 M in 0.1 N H_2SO_4), and taking into account the variable optical path lengths across the width of the cylindrical cell (see Appendix A). The I_0 values vary between 30 and 67 μeinstein $l^{-1}\ s^{-1}$. The derived Φ values are collected in Table 1.

Values of the pseudo-first-order constants k measured in air-saturated solutions ($[\mathrm{OClO}]_0 \approx 0.2$ mM) indicate a weak temperature dependence at all wavelengths between 250 and 316 K. For example, at 303 nm, such a dependence corresponds to an activation energy of about -1.1 ± 0.2 kcal mol^{-1}.

The influence of the photon irradiance on the photolysis rate was investigated by interposing fine mesh metal screens

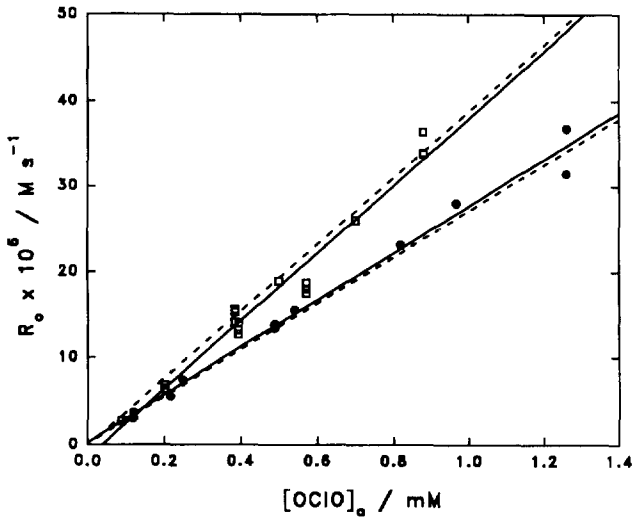

Fig. 7. As in Figs. 5 and 6, but at $\lambda = 303$ nm ($f = 1.13 \times 10^{-2}$ s^{-1}, $g = 1.20 \times 10^{-3}$ s^{-1}, $h = 9.89 \times 10^{-3}$ s^{-1}).

Table 1
Initial quantum yields of chlorine dioxide decay [a]

Quantum yield	$\lambda = 436$ nm	$\lambda = 365$ nm	$\lambda = 303$ nm
$\Phi(N_2)$	1.3	1.6	2.9
$\Phi(O_2)$	0.9	1.6	2.0
Φ(air)	0.9	1.7	2.3

[a] Calculated from Eq. (II).

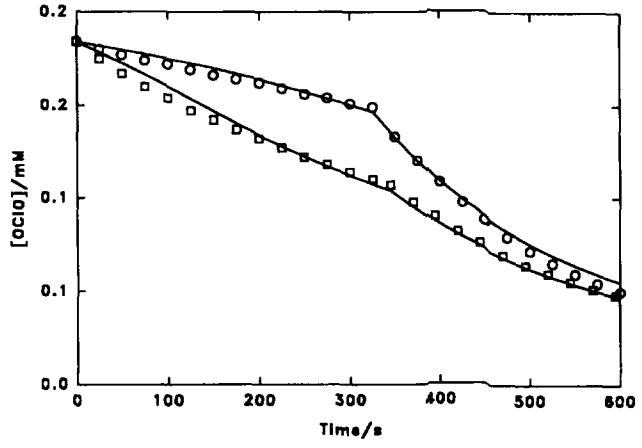

Fig. 8. [OClO] vs. time at $\lambda = 436$ nm: □, experimental data obtained on illumination initially attenuated by a 36.5% transmittance filter, which was removed at 350 s; ○, same as for □, but using a 12.9% transmittance filter removed at 320 s. Full lines correspond to simulated curves.

of known transmittance between the monochromator and the sample during irradiation. The ratio of the slopes about the break points, in conjunction with the ratio of the screen transmittances, allows the exponents n_i in $R \propto I_a^{n_i}$ to be determined (Fig. 8). A set of experiments with $[OClO]_0 = 0.3$ mM yielded $n_i = 0.99$ (436 nm), 0.95 (365 nm) and 0.94 (303 nm). The exponents n_i thus determined correspond to the actual dependence of the rates on the photon flux during the course of photolysis.

Molecular chlorine, a minor contaminant of our OClO solutions, can also be photolysed at some of the wavelengths used in these experiments [20]. In order to determine its influence on the kinetics of OClO photodecomposition, variable amounts of Cl_2 were purposely added to the solutions. In this manner, we verified that the presence of up to a 200% excess of Cl_2 relative to OClO did not detectably affect the initial rates at any wavelength.

Interestingly, on shutting off the irradiation of $[OClO]_0 = 13.3$ mM solutions at 365 nm and 298 K, the ESR signal slowly recovered, reaching a plateau after several minutes (see Fig. 4). Similar experiments carried out at 252 K (i.e. 2 K above the CCl_4 melting point) on previously purged frozen samples to eliminate overhead gaseous OClO led to the same result. In another experiment on a frozen solution at 233 K, after bleaching 99.8% of the initial ESR signal after 12 min of irradiation at 365 nm, a thaw and freeze cycle led to the recovery of 5% of the initial signal.

3.2. Mechanism

The ensuing discussion is based on the mechanism presented in Table 2. Numerical integration and parameter optimization were carried out using the FACSIMILE software package [28]. The $[O_2]$ values used in the calculations were estimated from Henry's law, $[O_2] = 11$ mM atm^{-1} $P(O_2)$, at 298 K, where $P(O_2)$ is the partial pressure of O_2 over the solutions [29]. Numerical values of the rate parameters in Table 2 were assessed by a self-consistent procedure involving:

Table 2
Mechanism of chlorine dioxide photolysis

Number	Reaction	Rate constant[a]
1	$OClO + h\nu \rightarrow ClO + O$	$f(I_0,\lambda)$[b]
2	$OClO + h\nu \rightarrow Cl + O_2$	$g(I_0,\lambda)$
3	$O + ClO \rightarrow Cl + O_2$	4.0×10^9
4	$O + OClO \rightarrow ClO_3$	2.0×10^9
5	$Cl + OClO \rightarrow ClO + ClO$	8.0×10^8
6	$ClO + ClO \rightarrow 2Cl + O_2$	5.0×10^6
7	$ClO + ClO \rightarrow OClO + Cl$	2.2×10^6
8	$ClO + ClO \rightarrow Cl_2 + O_2$	3.0×10^6
9	$O + O_2 \rightarrow O_3$	2.0×10^9
10	$Cl + O_3 \rightarrow ClO + O_2$	3.0×10^8
11	$ClO + ClO \rightarrow ClOOCl$	4.0×10^9
12	$ClOOCl \rightarrow ClO + ClO$	3.6×10^2
13	$OClO + ClO \rightarrow ClOClO_2$	4.0×10^9
14	$ClOClO_2 \rightarrow ClO + OClO$	7.0×10^3
15	$ClO_3 + ClO_3 \rightarrow Cl_2O_6$	1.0×10^9
16	$ClO_3 + ClO \rightarrow ClOClO_3$	1.0×10^9
17	$Cl + ClOOCl \rightarrow Cl + O_2 + Cl_2$	2.0×10^9
18	$Cl + ClOClO_2 \rightarrow ClO_3 + Cl_2$	2.0×10^9
19	$Cl + ClOClO_3 \rightarrow OClO + Cl_2 + O_2$	8.0×10^8
20	$O + OClO \rightarrow ClO + O_2$	6.0×10^7
21	$ClOClO_2 + h\nu \rightarrow ClO_3 + Cl$	$h(I_0,303$ nm)

[a] In CCl_4 (in M^{-1}s^{-1} units except f,g and h in s^{-1}) at 298 K.
[b] $R_1 = \varphi_{1\lambda} I_a = f[OClO]$. Similar expressions apply to R_2 and R_{21}. (See text and Appendix A.)

1. the initial estimation of rate constants based on gas phase values, when available, modified by phase transfer corrections;
2. the recognition of kinetic and/or thermodynamic constraints linking apparently independent parameters;
3. the assumption that radical–radical reactions are in principle diffusion controlled;
4. rounds of parameter optimization by fitting the mechanism to the experimental data of Figs. 1–3 and Figs. 5–7.

As indicated above, f, g and h, the rate constants of steps (1), (2) and (21), are implicit functions of the irradiation wavelength. Such a dependence involves the incident photon flux, the corresponding extinction coefficients and the primary quantum yields φ_λ. The φ_λ values are a measure of the escape probability of primary photofragments from the solvent cage, and as such must be smaller than unity [21,22]. Furthermore, h is related to $(f+g)$ via the ratio of the optical cross-sections of OClO and $ClOClO_2$ at 303 nm: $h/(f+g) = (\sigma_{ClOClO_2}/\sigma_{OClO})\varphi_{21}/(\varphi_1+\varphi_2)$ [20,25].

We set a bound of 4.0×10^9 M^{-1} s^{-1} to the maximum value of the rate constants of diffusion-controlled processes in CCl_4 solution [30]. It should be emphasized that the involvement of marginally stable intermediates in several reactions, such as (6)–(8) and (10), may possibly depress the net rates below the diffusion limit. Not all radical–radical reactions are truly independent. Thus the rate constants for the four channels of the bimolecular reaction (ClO + ClO) (steps (6)–(8) and (11)) must comply with the constraint $\Sigma k_{ClO+ClO} \le 4\times10^9$ M^{-1} s^{-1}, since they compete with each other in every encounter; as a consequence, their individual rate constants may fall below the diffusion-controlled limit for this reason alone. The same argument applies to reactions (4) and (20), which also compete. Radical equilibria must satisfy microreversibility via the corresponding thermochemical parameters [20]. The irreversible radical–radical bimolecular reactions (steps (3), (4), (9), (15) and (16)) as well as the presumably fast Cl atom abstractions (steps (17)–(19)) were assumed to be diffusion controlled at the outset.

The rate constants of many elementary reactions in Table 2 are known in the gas phase [20]. Their values in the liquid phase can be estimated by means of corrected equilibrium constants. More specifically, for the ratios $K_5 = k_7/k_5$, $K_{11} = k_{11}/k_{12}$ and $K_{13} = k_{13}/k_{14}$, we set the condition $1 < {}^{l}K_c/{}^{g}K_c < 100$, which was imposed as a restriction during parameter optimization [31].

There is always the question of whether a smaller mechanism could also have accounted for the experimental observations. Although there is not a general answer to this question, we wish to show that the proposed scheme is indeed minimal by focusing the analysis on the puzzling λ dependence of O_2 effects on the initial quantum yields (Table 1). Let χ be the branching ratio

$$\chi = f/(f+g) \qquad \text{(III)}$$

In the early stages of photolysis, step (1) must be followed by reaction of ClO and O-atoms with the major species initially present. Under an inert atmosphere ($[O_2]_0 = 0$), the only possible reactions are (O + OClO) and (ClO + OClO) (steps (4) and (13)). The overall stoichiometry of the {(1) + (4) + (13)} sequence corresponds to $3OClO + h\nu = ClO_3 + ClOClO_2$. In the presence of O_2 or air ($[O_2]_0 = 11$ mM and 2.3 mM respectively), O-atoms will preferentially react with O_2 via reaction (9), rather than with OClO via step (4). The stoichiometry of the sequence {(1) + (9) + (13)} is $2OClO + O_2 + h\nu = ClOClO_2 + O_3$.

A similar analysis can be made for the reactions following step (2), which only produces Cl atoms as reactive intermediates. In the absence or presence of O_2, Cl atoms will react with OClO producing two ClO radicals (step (5)), which will then engage in reaction (13). The net stoichiometry of {(2) + (5) + 2×(13)} is $4OClO + h\nu \rightarrow 2ClOClO_2 + O_2$. Summing up, step (1) destroys three OClO molecules under an inert atmosphere, but only two if O_2 is in excess initially. This is consistent with the behaviour observed at 436 and 303 nm (see Table 1). In contrast, step (2) destroys four OClO molecules per absorbed photon, regardless of whether there is O_2 in excess or not, a scenario which mimics the observations made at 365 nm.

A more detailed analysis provides quantitative information. The rate expressions for reactions (1) and (2) are

$$R_1 = f[OClO] = \varphi_{1\lambda} I_a \qquad \text{(IV)}$$

$$R_2 = g[OClO] = \varphi_{2\lambda} I_a \qquad \text{(V)}$$

where I_a is the (common) absorbed photon flux (einstein l^{-1} s^{-1}) and $\varphi_{1\lambda}$ and $\varphi_{2\lambda}$ are the corresponding primary quantum efficiencies. Considering that $\varphi_\lambda = \varphi_{1\lambda} + \varphi_{2\lambda} \le 1$ and $\chi = \varphi_{1\lambda}/\varphi_\lambda$

$$R_0(N_2) = 3R_1 + 4R_2 = (4-\chi)\varphi_\lambda I_a \qquad \text{(VI)}$$

$$R_0(O_2) = 2R_1 + 4R_2 = (4-2\chi)\varphi_\lambda I_a \qquad \text{(VII)}$$

Since, for dilute OClO solutions, I_a is directly proportional to [OClO], the experimental results of Figs. 5–7 are qualitatively accounted for. Regarding the phenomenological initial quantum yields Φ given in Table 1, we obtain from Eq. (VI) and Eq. (VII) at a given wavelength

$$\Phi(N_2)/\Phi(O_2) = (4-\chi)(4-2\chi) = \rho \qquad \text{(VIII)}$$

with $1 \le \rho \le 1.5$ depending on the branching ratio $0 \le \chi \le 1$. Table 3 summarizes the experimental and calculated parameters at different λ values under N_2 and O_2. The foregoing discussion shows that, in order to interpret the O_2 effects on the initial quantum yields, it is only necessary to invoke reactions (1), (2), (4), (5), (9) and (13), and assume that the branching ratio χ is a non-monotonic function of λ. The preceding conclusions are confirmed by numerical integration of the entire mechanism at conversions smaller than 5%.

At longer times, O_2 still continues to retard rates at 436 and 303 nm relative to the decays under N_2 (see Figs. 1 and 3). Cl atoms, formed in reactions (2), (3), (7) and (21) at 303 nm, where $ClOClO_2$ can be photolysed, participate in an autocatalytic chain reaction destroying OClO via steps (5)

Table 3
Wavelength dependence of the primary quantum yields of steps (1) and (2), and the O_2 effect on the overall quantum yields

	$\lambda = 436$ nm	$\lambda = 365$ nm	$\lambda = 303$ nm
$f(s^{-1})$	2.70×10^{-3}	7.27×10^{-3}	1.13×10^{-2}
$g(s^{-1})$	1.56×10^{-4}	1.94×10^{-2}	1.20×10^{-3}
χ [a]	0.95	0.27	0.90
$\rho(\exp)$ [b]	1.40	1.00	1.50
$\rho(\text{calc})$ [c]	1.40	1.08	1.41
$\varphi_\lambda(N_2)$ [d]	0.43	0.43	0.94
$\varphi_\lambda(O_2)$	0.43	0.46	0.91

[a] Calculated from Eq. (III).
[b] $\rho(\exp) = \Phi(N_2)/\Phi(O_2)$.
[c] $\rho(\text{calc}) = (4-\chi)/(4-2\chi)$.
[d] $\varphi_\lambda = \varphi_{1\lambda} + \varphi_{2\lambda}$.

and (6) [7]. Hence the rates are sensitive to the steady state [Cl] values and, as a consequence, to reactions that consume Cl atoms. Cl atoms are eliminated in steps (10), (18) and (19). Step (10) is the most important if O_3 is formed during reaction, because it introduces a delay in the autocatalytic removal of OClO. O_3 is produced by reaction (9) which, in turn, requires O atoms exclusively originating in reaction (1). If reaction (1) is inoperative, the overall reaction will proceed at a faster rate at all conversions, insensitive to the presence of added O_2. This is the behaviour found during photolysis at 365 nm. Finally, we tested whether the lack of an O_2 effect in Figs.2 and 6 was due to the relatively larger absorbed photon flux at 365 nm. A numerical experiment at 436 nm, in which f and g were increased tenfold relative to the value needed to simulate the data of Figs.1 and 5, indicated the persistence of lower rates under 1 atm O_2.

Despite the fact that parameter optimization leads to nearly unit quantum efficiency for radical escape in reactions (1) and (2) at 303 nm (Table 3), decay rates at 303 nm are underestimated unless the photolysis of $ClOClO_2$ also generates Cl atoms (step (21)). The optimized h values are consistent with $\sigma_{ClOClO_2} = 1.02 \times 10^{-18}$ cm^2 molecule^{-1} and $\varphi_{21} = 0.84$. Smaller h values result in slower overall initial rates, and increasingly poorer fits to the experimental data in Figs. 3 and 7.

The regeneration of OClO after the light is turned off still remains to be explained. Simulations of this phenomenon confirm the predictive power of the proposed mechanism: [OClO] increases by about 8% in the post-illumination period (see Fig. 4). The simulations also reveal that the maximum regeneration occurs if illumination is interrupted when the sum of the steady state [Cl] and [ClO] values reaches a maximum during the course of the run. In our mechanism, the dark reactions (7), (14) and (19) produce OClO. We found that there is no regeneration whatsoever if $k_{19} = 0$. Therefore chlorine perchlorate, the main stable product of OClO photolysis [7,12,32], acts as a pool from which OClO is recovered during the delayed release of ClO in step (14). Thus the simplest conceivable mechanism must provide for the formation of $ClOClO_3$ and $ClOClO_2$ to explain OClO regeneration. The partial recovery of OClO signals after melting bleached solid samples implies that O and Cl atoms and ClO radicals can diffuse in CCl_4 glasses.

Finally, it is reasonable to seek a plausible reason for the remarkable change in photoselectivity at 365 nm in solution, but not in the gas phase. As hinted above and elsewhere [15], kinematic cage effects will not suffice. Recently, we found that the sign and magnitude of the solvatochromic shifts undergone by OClO in a variety of solvents correlate with the Onsager function of their refractive indices [15]. By the same token, the static dielectric constants of the same solvents do not appreciably affect the energies of the electronic states involved in the transition responsible for the near-UV spectrum of OClO. The red shifts (relative to the gas phase) observed in all solvents therefore originate in the dynamic electronic polarization of the solvent, i.e. the solvent couples with the molecular manifold only during photon absorption [23]. After the transition is over, the system is left in a mixed state which could not have been reached by a dipolar transition of the isolated molecule. The intriguing possibility that the decay of such a uniquely prepared state might follow a different reaction pathway than those accessible in the gas phase within the same energy range deserves further study.

4. Conclusions

We present evidence that the photodissociation products of OClO dissolved in non-polar, polarizable CCl_4 solvent change from (ClO + O) at 303 and 436 nm to (Cl + O_2) at approximately 365 nm, at variance with the gas phase results. We emphasize the dependence of the solvatochromic shifts of OClO on the refractive indices rather than on the dielectric constants of the solvents involved, and suggest a possible relation to the mechanism of photoselectivity.

Acknowledgements

This project was financially supported by CONICET/Argentina under grant PID 1131/91. L.J.P. is a research staff member of CIC/Pcia. de Buenos Aires. A.J.C. is now at the Department of Physical Chemistry, Faculty of Exact and Natural Sciences, University of Buenos Aires.

Appendix A

To compare the photon fluxes through irradiated solutions of different refractive indices contained in cylindrical reactors, it is necessary to integrate the absorbances along the individual, non-parallel optical paths over the beam cross-section. This situation presents itself in the evaluation of the absorbed photon flux I_a by a CCl_4 solution ($n = 1.4601$) using incident photon fluences I_0 determined with an aqueous actinometer ($n = 1.338$). The derivation is straightforward [33] and

leads to $I_a = 240.8 I_0(303\ nm)[OClO]$, $I_a = 209.5 I_0(303\ nm)[ClOClO_2]$, $I_a = 803.9 I_0(365\ nm)[OClO]$ and $I_a = 196.6 I_0(436\ nm)[OClO]$ for 136 μl samples contained in 0.4 cm internal diameter tubes (I_a in M s^{-1}, I_0 in einstein l^{-1} s^{-1} and concentrations in M).

References

[1] V. Vaida and J.D. Simon, *Science, 268* (1995) 1443, and references cited therein.
[2] T. Baumert, J.L. Herek and A.H. Zewail, *J. Chem. Phys., 99* (1993) 4430.
[3] H.F. Davis and Y.T. Lee, *J. Phys. Chem., 96* (1992) 5681.
[4] W.G. Lawrence, K.C. Clemitshaw and V.A. Apkarian, *J. Geophys. Res. D, 95* (1990) 18 591.
[5] E.C. Richard and V. Vaida, *J. Chem. Phys., 94* (1991) 153.
[6] E. Bishenden and D.J. Donaldson, *J. Chem. Phys., 101* (1994) 9565.
[7] A.J. Colussi, *J. Phys. Chem., 94* (1990) 8922.
[8] A.J. Colussi, R.W. Redmond and J.C. Scaiano, *J. Phys. Chem., 93* (1989) 4783.
[9] R.C. Dunn and J.D. Simon, *J. Am. Chem. Soc., 114* (1992) 4856.
[10] R.C. Dunn, J.L. Anderson, C.S. Foote and J.D. Simon, *J. Am. Chem. Soc., 115* (1993) 5307.
[11] V. Vaida, S. Solomon, E.C. Richard, E. Ruhl and A. Jefferson, *Nature, 342* (1989) 405.
[12] F. Zabel, *Ber. Bunsenges. Phys. Chem., 95* (1991) 893.
[13] R.C. Dunn, B.N. Flanders, V. Vaida and J.D. Simon, *Spectrochim. Acta, Part A, 48* (1992) 1293.
[14] V. Vaida, K. Goudjil, J.D. Simon and B.N. Flanders, *J. Mol. Liq., 61* (1994) 133.
[15] M.S. Churio, M.A. Brusa, L.J. Perissinotti, E. Ghibaudi, M. Coronel and A.J. Colussi, *Chem. Phys. Lett., 232* (1995) 237.
[16] J.C. Mialocq, F. Barat, L. Gilles, B. Hickel and B. Lesigne, *J. Phys. Chem., 77* (1973) 742. H. Taube, *Trans. Faraday Soc., 53* (1957) 656.
[17] A. Arkell and I. Schwager, *J. Am. Chem. Soc., 89* (1967) 5999.
[18] F.J. Adrian, J. Bohandy and B.F. Kim, *J. Chem. Phys., 85* (1986) 2692.
[19] P. Raghunatan and S.K. Sur, *J. Am. Chem. Soc., 106* (1984) 8014.
[20] W.B. DeMore, S.P. Sander, C.J. Howard, A.R. Ravishankara, D.M. Golden, C.E. Kolb, R.F. Hampson, M.J. Kurylo and M.J. Molina, *Chemical Kinetics and Photochemical Data for Use in Stratospheric Modeling, JPL Publication 94-26*, Jet Propulsion Laboratory, California Institute of Technology, Pasadena, CA, 1994.
[21] K.B. Clark and D. Griller, *Chem. Phys. Lett., 168* (1990) 477.
[22] T. Koenig and H. Fischer, in J.K. Kochi (ed.), *Free Radicals*, Vol. 1, Wiley, New York, 1973, p. 157.
[23] E.G.J. McRae, *J. Phys. Chem., 61* (1957) 562.
[24] P. Suppan, *J. Photochem. Photobiol. A: Chem., 50* (1990) 293. D.M. Bishop, *Int. Rev. Phys. Chem., 13* (1994) 21.
[25] S.B. Burkholder, R.L. Mauldin, R.J. Yokelson, S. Solomon and A.R. Ravishankara, *J. Phys. Chem., 97* (1993) 7597.
[26] H.J. Kuhn, S.E. Braslavsky and R. Schmidt, *Pure Appl. Chem., 61* (1989) 187.
[27] P.W. Atkins, J.A. Brivati, N. Keen, M.C.R. Symons and P.A. Trevalion, *J. Chem. Soc.*, (1962) 4785.
[28] A.R. Curtis and W.P. Sweetenham, FACSIMILE: *A Computer Program for Flow and Chemistry Simulation and General Initial Value Problems*, UKAEA, Harwell, 1987.
[29] R. Battino (ed.), *Solubility Data*, Vol. 7, Pergamon, Oxford, 1981.
[30] J.I. Steinfeld, J.S. Francisco and W.L. Hase, *Chemical Kinetics and Dynamics*, Prentice Hall, Englewood Cliffs, NJ, 1989, p. 161.
[31] J.W. Moore and R.G. Pearson, *Kinetics and Mechanism*, Wiley, New York, 3rd edn., 1981, p. 246. J.M. Prausnitz, *Molecular Thermodynamics of Fluid-Phase Equilibria*, Prentice Hall, Englewood Cliffs, NJ, 1969, p. 271.
[32] A.J. Schell-Sorokin, D.S. Bethune, J.R. Lankard, M.M.T. Loy and P.P. Sorokin, *J. Phys. Chem., 86* (1982) 4653.
[33] M.S. Churio, *Doctoral Dissertation*, University of Mar del Plata, 1991.